Experimental Brain Research (2019) 237:161–171
https://doi.org/10.1007/s00221-018-5414-0

RESEARCH ARTICLE

Comparison of ion channel inhibitor combinations for limiting secondary degeneration following partial optic nerve transection

Lillian M. Toomey[1] · Carole A. Bartlett[1] · Maimuna Majimbi[2] · Gopana Gopalasingam[1] · Jennifer Rodger[1,3] · Melinda Fitzgerald[1,2,3]

Received: 11 April 2018 / Accepted: 21 October 2018 / Published online: 26 October 2018

Abstract

Following neurotrauma, secondary degeneration of neurons and glia adjacent to the injury leads to further functional loss. A combination of ion channel inhibitors (lomerizine + oxATP + YM872) has been shown to be effective at limiting structural and functional loss due to secondary degeneration. Here we assess efficacy of the combination where oxATP is replaced with Brilliant Blue G (BBG), a more clinically applicable $P2X_7$ receptor inhibitor. Partial optic nerve transection was used to model secondary degeneration in adult female rats. Animals were treated with combinations of lomerizine + YM872 + oxATP or lomerizine + YM872 + BBG, delivered via osmotic mini-pump directly to the injury site. Outcomes assessed were Iba1 + and ED1 + microglia and macrophages, oligodendroglial cell numbers, node/paranode structure and visual function using the optokinetic nystagmus test. The lomerizine + BBG + YM872 combination was at least as effective at the tested concentrations as the lomerizine + oxATP + YM872 combination at preserving node/paranode structure and visual function when delivered locally. However, neither ion channel inhibitor combination significantly improved microglial/macrophage nor oligodendroglial numbers compared to vehicle-treated controls. In conclusion, a locally delivered combination of ion channel inhibitors incorporating lomerizine + BBG + YM872 is at least as effective at limiting secondary degeneration following partial injury to the optic nerve as the combination incorporating oxATP.

Keywords Secondary degeneration · Neurotrauma · Ion channel inhibitor · Myelin · Visual function

Introduction

Following neurotrauma, a series of metabolic and structural changes are propagated in initially undamaged tissue, associated with increased intracellular Ca^{2+}, oxidative stress and apoptotic cell death of neurons and glia (Dong et al. 2009). Since the initial insult is often unavoidable, treatments for functional recovery after neurotrauma focus heavily on limiting this secondary damage (Doan et al. 2016). However, despite extensive research, effective pharmacotherapeutic treatments for secondary degeneration following neurotrauma are limited (Kwon et al. 2011). To successfully limit secondary degeneration following neurotrauma, it is important to test efficacy of treatments in appropriate animal models of injury. Partial optic nerve transection is an established and useful model for investigating secondary degeneration, where the dorsal optic nerve of adult rats is partially transected, allowing for spatial separation between the primary and subsequent secondary degeneration (Levkovitch-Verbin et al. 2003; Blair et al. 2005). The model has been further characterised and employed to assess efficacy of pharmacotherapeutics for secondary degeneration, delivered directly to the injury site using osmotic mini-pumps (Fitzgerald et al. 2009a, b; Savigni et al. 2013; Doig et al. 2017).

Secondary degeneration is characterised by a myriad of reactive metabolic pathways, including inflammation, excitotoxicity, mitochondrial dysfunction and oxidative stress, associated with structural deficits, dysmyelination and apoptotic cell death (Tymianski and Charles 1996; Dong

✉ Melinda Fitzgerald
lindy.fitzgerald@curtin.edu.au

1 Experimental and Regenerative Neurosciences, School of Biological Sciences, The University of Western Australia, 35 Stirling Hwy, Perth, WA 6009, Australia

2 Curtin Health Innovation Research Institute, Curtin University, Bentley, Australia

3 Perron Institute for Neurological and Translational Science, Sarich Neuroscience Research Institute Building, 8 Verdun St, Nedlands, WA 6009, Australia

et al. 2009; Maxwell 2013). Ca^{2+} overload is considered to be a major trigger for the toxic mechanisms of secondary degeneration (Farooqui et al. 2008). Using the partial optic nerve transection model, we have previously demonstrated that a locally delivered combinatorial treatment strategy to limit excess Ca^{2+} influx through voltage-gated calcium channels, $P2X_7$ receptors and Ca^{2+} permeable AMPA receptors with lomerizine, oxATP and YM872, respectively, reduced myelin decompaction, preserved node/paranode structure and visual function (Savigni et al. 2013). Acute outcomes indicated that early preservation of node/paranode structure and OPC numbers was associated with longer term preservation of visual function (Doig et al. 2017).

Following mild traumatic brain injury, it is currently unclear as to whether there is a blood–brain barrier breach, with studies reporting varying degrees of compromise of blood–brain barrier integrity following injury (Deford et al. 2002; Tomkins et al. 2011; Zetterberg et al. 2013). Therefore, pharmacotherapies designed to treat all but the most severe cases of neurotrauma, need to be able to travel across the closed blood–brain barrier following systemic delivery. oxATP does not appear to be able to cross the blood–brain barrier (Peng et al. 2009). Thus, for clinical applicability of the lomerizine, oxATP and YM872 combination, oxATP needs to be substituted with a blood–brain barrier permeable $P2X_7$ receptor antagonist. Here we introduce an alternative $P2X_7$ receptor inhibitor Brilliant Blue G (BBG) to the combination. BBG has previously shown therapeutic effects following neurotrauma (Peng et al. 2009; Kimbler et al. 2012; Wang et al. 2015), and importantly, can cross the closed blood–brain barrier (Wong et al. 2011). This study compared the efficacy of the ion channel inhibitor combination of lomerizine + BBG + YM872 to a combination with lomerizine + oxATP + YM872 for limiting secondary degeneration and restoring function following partial optic nerve transection.

Methods

Animals and study design

Thirty-eight adult, female PVG rats were obtained from the Animal Resource Centre in Murdoch, Western Australia. The animals were housed under 12-h light/dark cycles with ad libitum access to food and water. All procedures were approved by the University of Western Australia Animal Ethics Committee (approval number RA3/100/1485) and were in accordance with the National Health and Medical Research Council (NHMRC) of Australia Code of Practice for use of Animals for Scientific Purposes. The animals were divided into four experimental groups, a sham-injured, vehicle-treated group ($n = 8$); an injured, vehicle-treated group ($n = 10$); an injured, lomerizine + oxATP + YM872-treated group ($n = 10$); and an injured, lomerizine + BBG + YM872-treated group ($n = 10$); with the sham group serving as an uninjured, vehicle-treated control.

Surgical procedures

Partial optic nerve transection (day 1) and left eyelid suturing (day 3) were performed as previously described (Fitzgerald et al. 2009a), under ketamine (ketamil, 50 mg/kg, Troy Laboratories) and xylazine (Ilium Xylazil, 10 mg/kg, Troy Laboratories) anaesthesia administered intraperitoneally. In brief, for the partial transection surgery: the skin overlying the skull behind the right eye was incised. The optic nerve was accessed and the nerve parenchyma exposed by making a longitudinal cut in the sheath using fine iridectomy scissors. About 1 mm behind the right eye, the dorsal aspect of the optic nerve was partially lesioned to a depth of approximately 200 µm with a diamond radial keratotomy knife (Geuder); the depth determined by the protrusion of the blade beyond the surrounding guard. Sham injury included all procedures except the cut in the sheath and the partial optic nerve lesion. Surgical implantation of Alzet osmotic mini-pumps was performed as described (Savigni et al. 2013). Immediately following surgery, subcutaneous injections of analgesia (2.8 mg/kg carprofen, Norbrook) and 1 mL sterile phosphate buffered saline (PBS) were administered.

Treatments

Lomerizine (30 mg/kg, LKT Labs©) was orally administered in butter vehicle twice daily 8 h apart, until end of the experiment, commencing once animals were ambulatory following surgery as previously described (Fitzgerald et al. 2009a). oxATP (1 mM), BBG (540 µM) and YM872 (240 µM) were delivered via osmotic mini-pump at 0.5µL/h in PBS vehicle. Concentrations employed for oxATP and YM872 were consistent with our previous studies where efficacy was demonstrated (Savigni et al. 2013), and the BBG dose was chosen with reference to the literature describing efficacy of BBG and YM872 in related models (Takahashi et al. 2002; Diaz-Hernandez et al. 2012; Cervetto et al. 2013). The sham-injured and partial optic nerve transection injured, vehicle-treated experimental groups both received PBS via osmotic mini-pump and butter orally, administered as described for the inhibitor-treated groups.

Behavioural assessment

On day 3, the animals were anaesthetised as described above and their uninjured left eyelids sutured shut. The optokinetic nystagmus assessment of visual function was performed on

day 4 for all animals, in accordance with established procedures (Fitzgerald et al. 2010b). Animals were videoed and the number of responses per unit time engaged in the task was determined by a single investigator blinded to animal identity. Note that due to a procedural error, $n = 5$ for the injured, vehicle-treated group. Responses were categorised as either smooth pursuits or fast resets. Smooth pursuits are characterised as an elongated head rotation tracking the stripes, and fast resets as a rapid, realigning head movement; both elements are an indication of visual ability of the animal (Abdeljalil et al. 2005).

Tissue processing and immunohistochemistry

Immediately following behavioural assessment, rats were euthanised with pentobarbitone sodium (160 mg/kg, Delvet), transcardially perfused with 0.9% saline, followed by 4% paraformaldehyde (Sigma-Aldrich) in 0.1M PBS. Optic nerves were dissected and fixation continued overnight by immersion in 4% paraformaldehyde. Tissue was transferred into 15% sucrose (Chem Supply) in PBS, then cryosectioned in longitudinal orientation at a thickness of 14 µm and collected onto Superfrost Plus glass microscope slides. Immunohistochemistry was conducted in accordance with established procedures (Fitzgerald et al. 2010a) using primary antibodies recognising: microglial activation markers Iba1 (1:500; Abcam, goat Ab5076) and ED1 (1:500; Merck Millipore, mouse MAB1435); oligodendroglial indicators oligodendrocyte transcription factor 2 (Olig2; 1:500; R&D Systems, goat AF2418) and platelet-derived growth factor alpha receptor (PDGFαR; 1:500; Abcam Ab96806); and for paranode and node of Ranvier structures Caspr (1:500; Abcam, rabbit Ab34151), and β-III tubulin (1:500; Merck Millipore, mouse MAB1637). Antibodies were diluted in PBS containing 0.2% Triton™ X-100 and 5% normal donkey serum. Secondary antibodies were Alexa Flour 488 or 555 (1:400; Thermo Fisher Scientific™), together with Hoechst 3342 (1:1000; Thermo Fisher Scientific™) diluted in PBS containing 0.2% Triton™ X-100. Finally, the sections were mounted and cover slipped using Fluoromount-G (Thermo Fisher Scientific).

Imaging and analysis

The ventral optic nerve directly below the site of injury was visualised, with one field of view from one section per animal imaged for each outcome measure. The slides were viewed using either a Nikon Ni-E confocal fluorescence microscope (Nikon Corporation) or a Nikon Eclipse Ti-inverted microscope. A series of 13 optical images were taken at 0.5 µm increments along the z axis, and deconvoluted using Nikon Elements AT software. Imaging for each outcome measure was performed in a single sitting with consistent capture settings. All image analysis was performed on Fiji image processing software (NIH) by a single investigator blinded to section identity. Due to poor fixation and tissue processing in a few animals, the number of animals per group analysed for immunohistochemistry outcomes were: sham-injured, vehicle-treated group ($n = 8$); injured, vehicle-treated group ($n = 10$); injured, lomerizine + oxATP + YM872-treated group ($n = 8$); and injured, lomerizine + BBG + YM872-treated group ($n = 9$).

Total numbers of Iba1+ resident reactive microglia, ED1+ activated microglia/macrophages, Olig2+ oligodendroglia and Olig2+/PDGFαR+ oligodendrocyte precursor cells (OPCs) were counted within a region of interest in a 20 × image of the ventral nerve directly beneath the primary injury site and expressed as the mean number of cells/mm^2. For node/paranode analyses, a single 60 × z stack image per animal was divided into a 3 × 3 grid and all complexes with clearly defined Caspr immunostaining in a single randomly selected grid square assessed; at least 30 node/paranode complexes were analysed per animal. Outcome measures were the length of the paranodal gap, defined as the distance between two Caspr+ areas; paranode length, as defined by the length of Caspr+ areas; and the percentages of atypical nodal complexes, as previously described (Szymanski et al. 2013).

Statistics

Results were analysed using IBM SPSS software. Outliers were detected using the Tukey's outlier detection model, whereby data that were greater than 1.5 interquartile ranges outside of the first and third quartiles were considered outliers and removed from the data set. No more than two outliers were removed per treatment group for each outcome measure, details are provided in figure legends. A single one-way ANOVA encompassing all four treatment groups were performed for each outcome measure. Normality was assumed, Levene's test was used to assess homogeneity of variances for each data set ($\alpha = 0.05$). If Levene's test showed equal variance, the Tukey post hoc test was used; for unequal variance, the Games-Howell post hoc test was applied; both used $p \leq 0.05$ to indicate statistical significance.

Results

Effects of ion channel inhibitor combinations on microglia and macrophages

Numbers of inflammatory cells in ventral optic nerve vulnerable to secondary degeneration were quantified using Iba1 for resident microglia, ED1 for infiltrating microglia/macrophages, and colocalised Iba1+/ED1+ for infiltrating

microglial cells (Wu et al. 2005). The numbers of Iba1+ activated resident microglia were different in the various treatment groups (Fig. 1a, $F = 3.483$, $df = 3$, $p = 0.028$), with the only statistically significant difference an increase in the number of Iba1+ cells when animals were treated with lomerizine + BBG + YM872 compared to the sham-injured, vehicle-treated group ($p = 0.029$). There was a trend towards increased Iba1+ cells with injury when comparing the injured, vehicle-treated group with the sham-injured, vehicle-treated group ($p = 0.071$). There was no significant difference between the two ion channel inhibitor combinations in the number of Iba1+ cells ($p = 0.938$).

In contrast, there was a significant difference in numbers of ED1+ infiltrating microglia/ macrophages (Fig. 1b, $F = 2.5$, $df = 3$, $p = 0.079$), with the numbers of the injured, vehicle-treated group significantly increased compared to sham-injured, vehicle-treated animals ($p = 0.049$). The number of ED1+ cells in the groups treated with either of the ion channel inhibitor combinations was not significantly different to either the injured, vehicle-treated group or the sham-injured, vehicle-treated group ($p > 0.05$). There was no significant difference between the two ion channel inhibitor combinations in the number of ED1+ cells ($p = 0.994$).

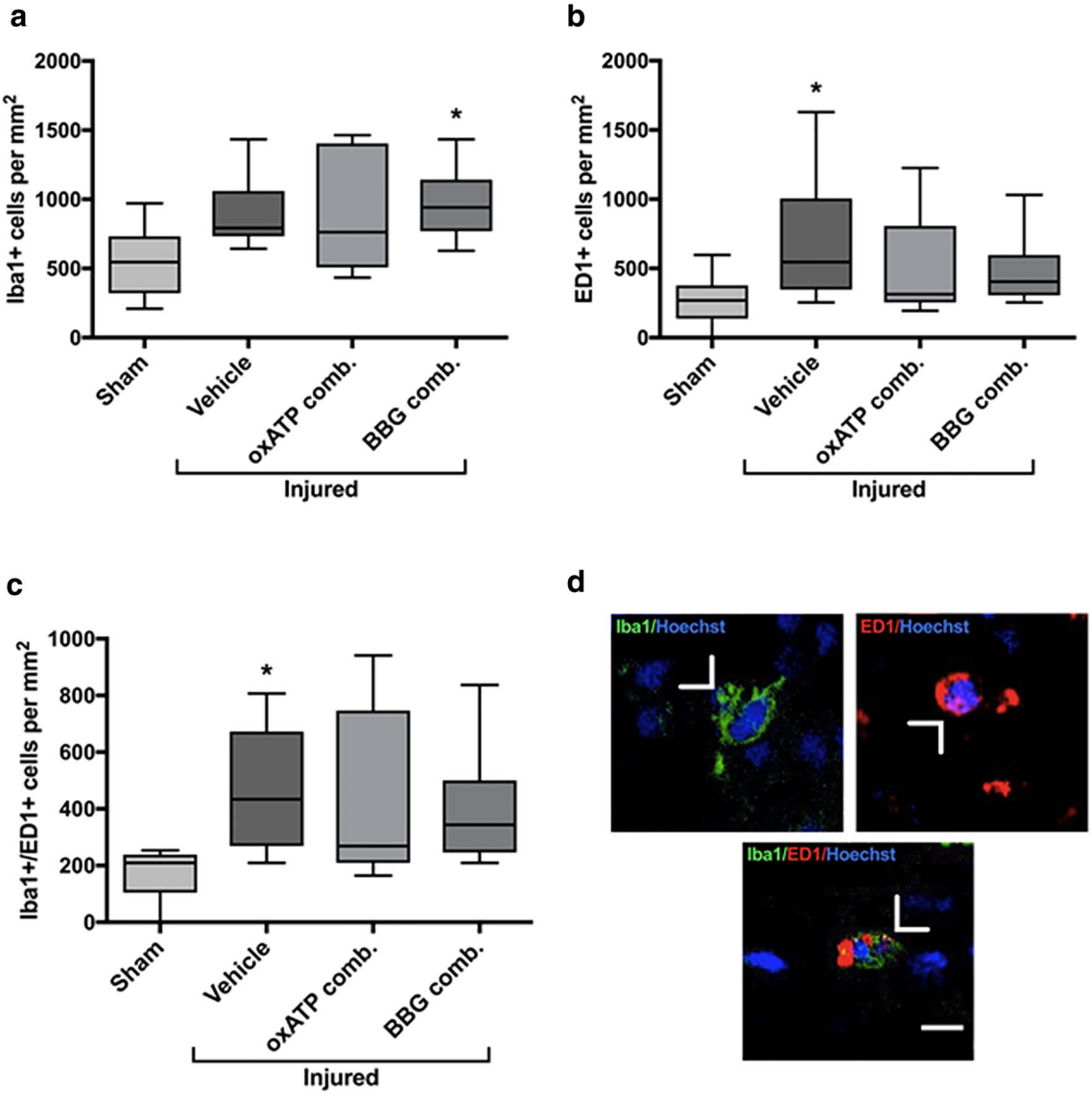

Fig. 1 Effects of ion channel inhibitor combinations on densities of Iba1+ and ED1+ cells. Densities of Iba1+ (**a**), ED1+ (**b**) and Iba1+/ED1+ (**c**) cells in the ventral optic nerve from sham-injured, vehicle-treated animals, injured, vehicle-treated animals, and ion channel inhibitor-treated animals 3 days after partial optic nerve transection. $N = 7$–10 rats per group; graphs display min to max values, with the central line representing the median data point. Significant differences compared to sham are indicated by $^*p \leq 0.05$. **d** Representative images of Iba1+, ED1+ and Iba1+/ED1+ cells, indicated with arrow heads; scale bar 10 µm

Similarly, the number of Iba1+/ED1+ infiltrating microglial cells differed with experimental treatment (Fig. 1c, $F = 2.912$, $df = 3$, $p = 0.041$). A significant increase in the numbers of Iba1+/ED1+ cells was observed in the injured, vehicle-treated group compared to the sham-injured, vehicle-treated group ($p = 0.024$). Neither of the ion channel inhibitor treatment groups had significantly reduced numbers of Iba1+/ED1+ cells compared to the injured, vehicle-treated group ($p > 0.05$). There was no significant difference between the two ion channel inhibitor combinations in the number of Iba1+/ED1+ cells ($p = 0.988$). Representative images of Iba1+ cells, ED1+ cells and Iba1+/ED1+ cells are shown (Fig. 1d).

Effects of ion channel inhibitor combinations on oligodendroglia

The densities of Olig2+ oligodendroglia were not different in any of the experimental groups (Fig. 2a, $F = 2.042$, $df = 3$, $p = 0.128$); an example cell is shown (Fig. 2b). However, when the analysis was refined to include immunoreactivity to PDGFαR, thereby detecting OPCs more

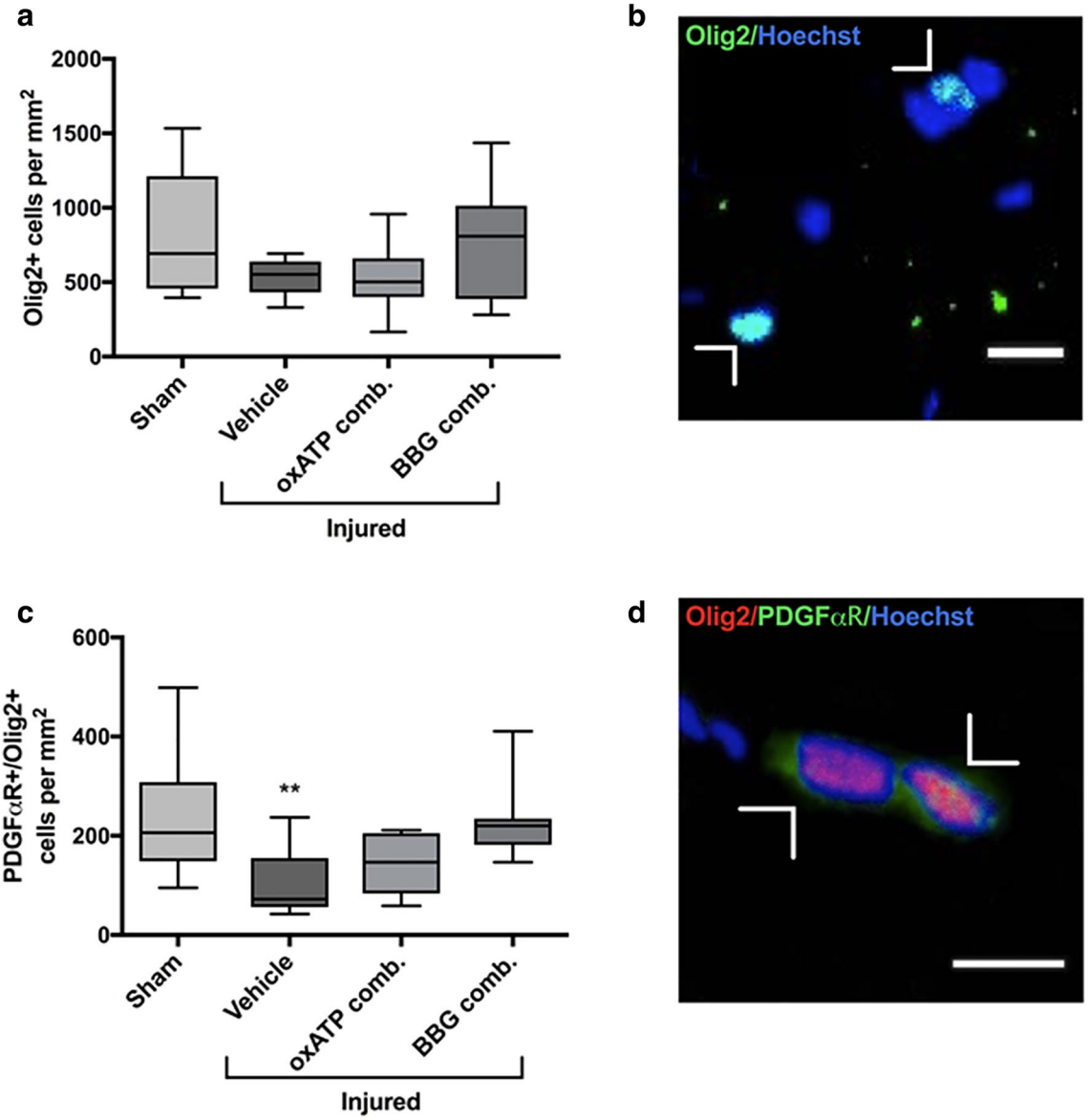

Fig. 2 Effects of ion channel inhibitor combinations on oligodendroglial cells. Densities of Olig2+ oligodendroglial cells (**a**) and PDGFαR+/Olig2+ OPCs (**c**) in the ventral optic nerve from sham-injured, vehicle-treated animals, injured, vehicle-treated animals, and ion channel inhibitor-treated animals, 3 days after partial optic nerve transection. $N = 8$–10 rats per group. Graphs display min to max values, with the central line representing the median data point. Significant differences compared to sham are indicated by $^{**}p \leq 0.01$. Representative image of Olig2+ cells (**b**) and OPCs (**d**), indicated with arrow heads; scale bar 15 µm and 10 µm respectively

specifically, there were significant differences between experimental groups (Fig. 2c, d, $F = 4.681$, $df = 3$, $p = 0.008$). As expected (Doig et al. 2017), there was a significant decrease in the number of OPCs in the injured, vehicle-treated group compared to the sham-injured, vehicle-treated group ($p = 0.007$). However, neither ion channel inhibitor combination groups had significantly increased numbers of OPCs compared to the injured, vehicle-treated group ($p > 0.05$), and there was no significant difference between the two ion channel inhibitor combinations in the number of OPCs ($p = 0.599$).

Effects of ion channel inhibitor combinations on node/paranode complexes

Significant differences in the length of the paranode between experimental groups were observed (Fig. 3a, $F = 52.445$, $df = 3$, $p = 0.0001$). Partial optic nerve transection resulted in a significant increase in paranode length in the injured, vehicle-treated group compared to the sham-injured, vehicle-treated group ($p = 0.0001$), as expected from previous studies (Szymanski et al. 2013). While treatment with lomerizine + oxATP + YM872 reduced paranode

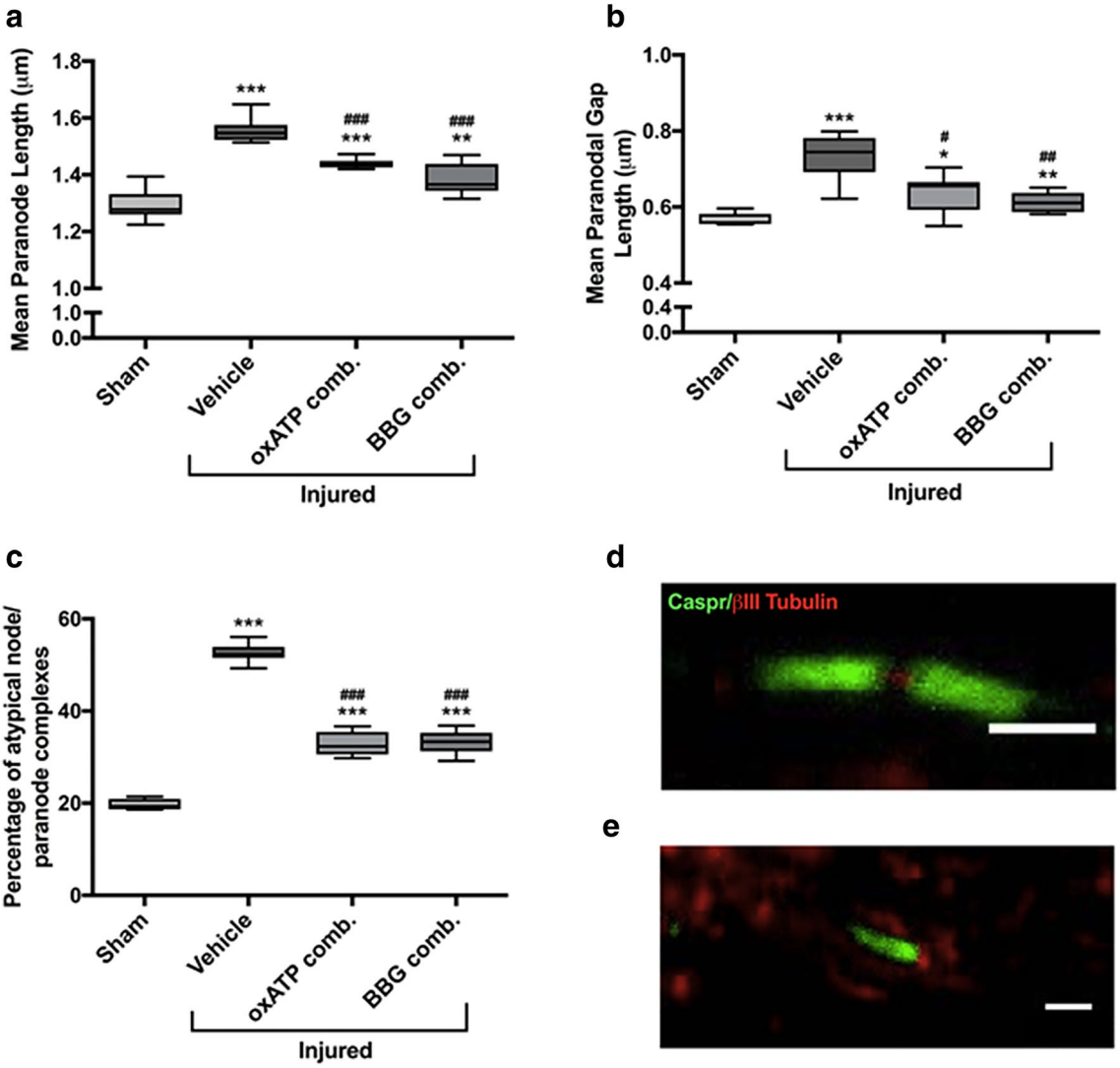

Fig. 3 Effect of ion channel inhibitor combinations on node/paranode complexes. Paranode length (**a**), paranodal gap length (**b**) and percentage of atypical node/paranode complexes (**c**) from 30 nodal complexes per animal in the ventral optic nerve from sham-injured, vehicle-treated animals, injured, vehicle-treated animals, and ion channel inhibitor-treated animals 3 days after partial optic nerve transection. Graphs display min to max values, with the central line representing the median data point; $N = 6$–9 rats per group. Significant differences indicated by $^{*}p \leq 0.05$, $^{**}p \leq 0.01$, and $^{***}p \leq 0.001$. Differences compared to the sham-injured, vehicle-treated group are indicated by *, similarly, differences compared to the injured, vehicle-treated group are indicated by #. **d** Representative image of two Caspr+ areas flanking a β-III tubulin+ area i.e. a typical nodal complex; scale bar 2 µm. **e** Representative image of one Caspr+ area flanking a β-III tubulin+ area denoting an atypical nodal complex/heminode; scale bar 2 µm

length ($p = 0.0001$), paranodes remained longer than in the sham-injured, vehicle-treated group ($p = 0.0001$). Treatment with the lomerizine + BBG + YM872 combination also resulted in significantly reduced paranode lengths compared to the injured, vehicle-treated group ($p = 0.0001$), to levels significantly different to the sham-injured, vehicle-treated group ($p = 0.001$). Largely similar outcomes were observed when measuring the length of the paranodal gap, indicative of the length of the node of Ranvier (Fig. 3b, $F = 20.367$, $df = 3$, $p = 0.0001$). There was no significant difference between the two ion channel inhibitor combinations in the length of the paranode ($p = 0.084$) or the paranodal gap ($p = 0.122$).

There were significant differences between experimental groups in the percentage of atypical nodal complexes (Fig. 3c–e, $F = 374.951$, $df = 3$, $p = 0.0001$). Atypical nodal complexes were defined as either a heminode, characterised as a β-III tubulin+ area flanked by only one Caspr+ area (Fig. 3e), or a single paranode, defined as a Caspr+ area not associated with a β-III tubulin + area (Szymanski et al. 2013). Injury resulted in an increase in the percentage of atypical nodal complexes in the injured, vehicle-treated group compared to the sham-injured, vehicle-treated group ($p = 0.0001$), which was significantly reduced by both lomerizine + oxATP + YM872 ($p = 0.0001$) and lomerizine + BBG + YM872 ($p = 0.0001$). However, both ion channel inhibitor combination groups still had significantly increased levels of atypical nodal complexes compared to the sham-injured, vehicle-treated group ($p = 0.0001$). There was no significant difference between the two ion channel inhibitor combinations in the number of atypical nodal complexes ($p = 0.668$).

Effects of ion channel inhibitor combinations on the optokinetic nystagmus reflex

The optokinetic nystagmus test of visual function revealed significant differences in the number of smooth pursuits and fast resets following injury and treatment (Fig. 4a; smooth pursuits $F = 7.05$, $df = 3$, $p = 0.001$; fast resets $F = 7.656$, $df = 3$, $p = 0.001$). Injury resulted in a significant decrease in the numbers of both smooth pursuits and fast resets by the injured, vehicle-treated group compared to the sham-injured, vehicle-treated group ($p = 0.002$, $p = 0.001$, respectively). Animals treated with lomerizine + oxATP + YM872 made significantly more smooth pursuits than the injured, vehicle-treated group ($p = 0.035$), but fewer fast resets than the sham-injured, vehicle-treated group ($p = 0.006$). Animals treated with lomerizine + BBG + YM872 made significantly more smooth pursuits ($p = 0.002$) and fast rests ($p = 0.039$) than the injured, vehicle-treated group; outcomes were not different from the sham-injured, vehicle-treated group ($p = 0.992$, $p = 0.284$, respectively). There was no significant difference between the two ion channel inhibitor combinations in the number of smooth pursuits ($p = 0.422$) or fast resets ($p = 0.222$).

To control for the length of the tracking motions, the time spent engaging in tracking behaviour was also assessed, giving similar outcomes (Fig. 4b, $F = 11.458$, $df = 3$, $p = 0.0001$). Injury resulted in a significantly lower proportion of time spent engaging in smooth pursuits by the injured, vehicle-treated group compared to the sham-injured, vehicle-treated group ($p = 0.0001$). Animals treated with lomerizine + oxATP + YM872 spent more time tracking than the injured, vehicle group ($p = 0.01$), but still less time

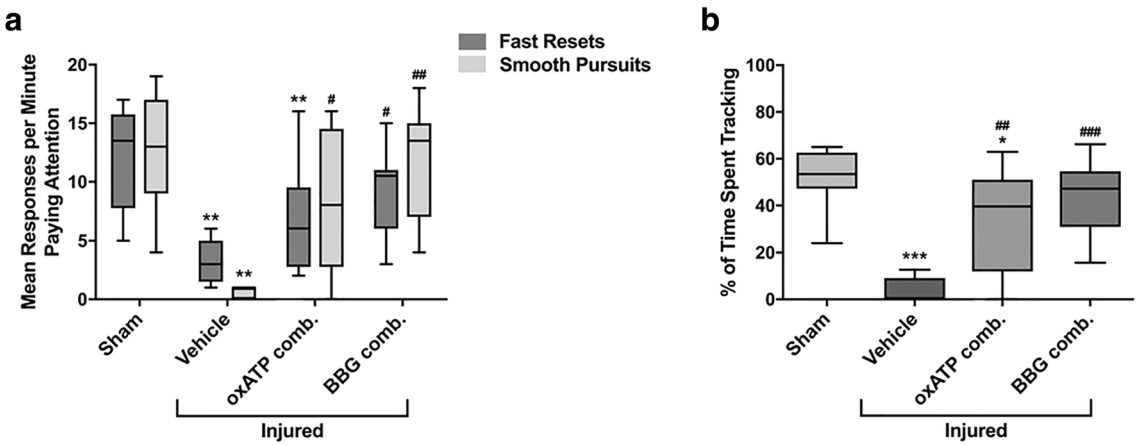

Fig. 4 Effects of injury and ion channel inhibitor combinations on the number of responses in the optokinetic nystagmus test of visual function. Total number of smooth pursuits and fast resets per minute engaged in the task (**a**) and proportion of time paying attention to task engaged in smooth pursuits (**b**) by sham-injured, vehicle-treated animals; injured, vehicle-treated animals; or injured ion channel inhibitor-treated animals. Graphs display min to max values, with the central line representing the median data point; $N = 5$–10 rats per group. Significant differences are indicated by $^{*}p \leq 0.05$, $^{**}p \leq 0.01$, and $^{***}p \leq 0.001$. Differences compared to the sham-injured, vehicle-treated group are indicated by *, differences compared to the injured, vehicle-treated group are indicated by #

than the sham-injured, vehicle-treated group ($p = 0.045$). Animals treated with lomerizine + BBG + YM872 also spent significantly longer performing smooth pursuits than the injured, vehicle-treated group ($p = 0.0001$), and the time spent tracking was not significantly different to the sham-injured, vehicle-treated group ($p = 0.161$). There was no significant difference between the two ion channel inhibitor combinations in the time spent tracking ($p = 0.601$).

Discussion

The aim of this study was to determine if the combination of lomerizine + oxATP + YM872, shown to effectively limit functional loss associated with secondary degeneration of the optic nerve (Savigni et al. 2013), would be as effective if oxATP was replaced with BBG, a more clinically applicable $P2X_7$ receptor inhibitor that can cross the closed blood–brain barrier. It was found that the lomerizine + BBG + YM872 combination was as effective, or marginally more effective at the tested concentrations, than the lomerizine + oxATP + YM872 combination, at preserving node/paranode structure and visual function when delivered locally. However, neither therapeutic combination affected numbers of microglia and macrophages, or the number of OPCs or oligodendrocytes. The data suggest an associative relationship between preservation of myelin structure and maintenance of visual function following injury.

The observed increase in nodal and paranodal lengths following partial optic nerve injury is in line with previous findings (Szymanski et al. 2013; Doig et al. 2017) and is suggestive of myelin retraction and a breakdown of the paranodal junction (Arancibia-Carcamo and Attwell 2014). Increased $P2X_7$ receptor activation on the myelin sheath has also been associated with myelin degradation following injury, however the underlying cellular mechanisms remain unclear (Matute 2008). The lomerizine + BBG + YM872 combination restored nodal and paranodal structure to dimensions slightly closer to the sham control group than the lomerizine + oxATP + YM872 combination. The lomerizine + BBG + YM872 combination was the only treatment to not be different to the sham control group for visual function. BBG is a more potent and selective antagonist of $P2X_7$ receptors than oxATP (Donnelly-Roberts and Jarvis 2007), which may explain this marginally greater efficacy of the BBG containing combination in preserving myelin structure and visual function compared to the control groups in the current study. However, titration of doses of these agents relative to their specific inhibitory concentrations for $P2X_7$ receptors is required to definitively compare efficacy of the two agents within the context of this treatment combination and injury model. We have previously established that locally delivered oxATP alone does not preserve node/paranode structure nor visual function in the partial optic nerve transection model (Savigni et al. 2013). The addition of lomerizine and YM872 to the combination is required for full beneficial effects (Savigni et al. 2013), emphasising that limiting excess Ca^{2+} flux through voltage-gated calcium channels and Ca^{2+} permeable AMPA receptors is also important.

Following injury to the CNS, there is a high influx of Ca^{2+} into myelin via AMPA receptors (Fowler et al. 2003), which results in increased Ca^{2+} binding to the catalytic core of calpain, enhancing calpain activation (Croall and Demartino 1991; Khorchid and Ikura 2002). An increase in calpain activation can induce myelin degradation, via cleavage of myelin basic protein and myelin-associated glycoprotein (Banik et al. 1985; Shields et al. 1997; Fu et al. 2007). Myelin degradation has been associated with paranodal loop eversion and sheath retraction and thus increased nodal and paranodal lengths (Ouyang et al. 2010). Therefore, observed preservation of nodal and paranodal length by both ion channel combinations may be due to inhibition of this Ca^{2+}-dependent calpain mechanism through the antagonistic activity of YM872 on AMPA receptors.

Furthermore, when the axolemma becomes exposed following myelin sheath retraction, and paranodal splitting, there is an increase in Ca^{2+}entry into axons via sub-myelin L-type VGCCs, which are normally hidden underneath the myelin sheath (Zhang and David 2015). This contributes to neuronal Ca^{2+} overload, associated with oxidative stress, caspase-mediated apoptosis and decreased function (Annunziato et al. 2003). Lomerizine-mediated inhibition of these sub-myelin VGCCs from beneath the sheath, together with exposure of fewer L-type VGCCs by prevention of the myelin retraction, may be a further therapeutic mechanism of the combinations of inhibitors.

Myelin structure is integral to the capacity of nerves to propagate action potentials, with the lengthening of the node associated with slower conduction velocities in a variety of pathologies (Howell et al. 2006; Reimer et al. 2011; Sun et al. 2012). Abnormal myelination at a single internode can be sufficient to block neural signal transduction for an entire axon (Baumann and Pham-Dinh 2001). Previous studies have also hypothesised that abnormalities in the node of Ranvier proteins, associated with increased nodal length, may result in decreased synchronicity of neuronal firing (Arancibia-Carcamo and Attwell 2014). Preservation of myelin integrity by the ion channel inhibitor combinations may be facilitating action potential propagation along axons, associated with preservation of function following injury.

However, in the current study, myelin structure and visual function were only partly preserved by the ion channel inhibitor treatments, which suggest some aspects of myelin breakdown following injury are mediated via alternative mechanisms of damage. One potential mechanism

is immune cell-mediated depletion of OPCs. The current study found that following injury, there is a significant increase in infiltrating microglia and macrophages, but not resident microglial cells, indicative of an infiltrating immune response. However, treatment did not show a significant effect at ameliorating this infiltrating immune response. Following neurotrauma, inflammatory cells produce cytokines and chemokines, as well as reactive oxygen species, resulting in oxidative damage of surrounding tissue (Anderson 2002). OPCs are especially vulnerable to oxidative stress and apoptosis following injury (Thorburne and Juurlink 1996; Giacci et al. 2018), which may be why the combinations of ion channel inhibitors were unable to ameliorate the loss of OPCs in this study. OPCs are required for oligodendrogenesis and remyelination following injury (Mirron et al. 2011). OPCs also contribute to the formation of myelin nodal structures (Butt et al. 2004). It may be that significantly preserving OPCs following injury, perhaps through preventing this infiltrating immune response, would be associated with a complete preservation of myelin structure and thus visual function. Furthermore, given previous studies have found an increased therapeutic effect of the lomerizine + oxATP + YM872 combination after 3 months of administration compared to 3 days (Savigni et al. 2013; Doig et al. 2017), it may be that a longer duration of treatment would provide further improvements to these outcomes following injury.

This study showed that the combination of lomerizine + BBG + YM872, which has the potential to be delivered systemically following injury, shows promise for limiting secondary degeneration following neurotrauma, however further work remains to be done. While BBG is a highly selective $P2X_7$ receptor antagonist, it is 30–50 times more potent in rats than humans (Jiang et al. 2000), which will necessitate careful titration of dosages before clinical translation will be feasible. Lomerizine is currently used in clinical practice (Hara et al. 1999), YM872 is more soluble than other Ca^{2+} permeable AMPA receptor inhibitors (Takahashi et al. 2002) and has been trialled in stroke with an acceptable safety profile (Labiche and Grotta 2004) and BBG has a no-observed-adverse-effect level of 8966 mg/kg per day in a mouse model of lifetime toxicity (Borzelleca et al. 1990). Nevertheless, while no adverse effects have been observed in our rodent model, the combination of three ion channel inhibitors will need to be careful assessed for toxicity in humans before a trial of efficacy following neurotrauma can be contemplated. Furthermore, given the clinical need for systemically administered drug delivery following neurotrauma, the efficacy of this blood–brain barrier permeable combination of lomerizine + BBG + YM872 needs to be tested when systemically delivered following injury.

Acknowledgements MF is supported by an NHMRC Career Development Fellowship (APP1087114).

Compliance with ethical standards

Conflict of interest The authors declare that they have no conflict of interest.

References

Abdeljalil J, Hamid M, Abdel-Mouttalib O et al (2005) The optomotor response: a robust first-line visual screening method for mice. Vis Res 45:1439–1446. https://doi.org/10.1016/j.visres.2004.12.015

Anderson A (2002) Mechanisms and pathways of inflammatory responses in CNS trauma: spinal cord injury. J Spinal Cord Med 25:70–79

Annunziato L, Amoroso S, Pannaccione A et al (2003) Apoptosis induced in neuronal cells by oxidative stress: role played by caspases and intracellular calcium ions. Toxicol Lett 139:125–133. https://doi.org/10.1016/S0378-4274(02)00427-7

Arancibia-Carcamo I, Attwell D (2014) The node of Ranvier in CNS pathology. Acta Neuropathol 128:161–175. https://doi.org/10.1007/s00401-014-1305-z

Banik NL, McAlhaney WW, Hogan EL (1985) Calcium-stimulated proteolysis in myelin: evidence for a Ca^{2+}-activated neutral proteinase associated with purified myelin of rat CNS. J Neurochem 45:581–588. https://doi.org/10.1111/j.1471-4159.1985.tb04026.x

Baumann N, Pham-Dinh D (2001) Biology of oligodendrocyte and myelin in the mammalian central nervous system. Physiol Rev 81:871–927

Blair M, Pease ME, Hammond J, Valenta D, Kielczewski J, Levkovitch-Verbin H, Quigley H (2005) Effect of glatiramer acetate on primary and secondary degeneration of retinal ganglion cells in the rat. Investig Opthalmol Vis Sci 46:884–884. https://doi.org/10.1167/iovs.04-0731

Borzelleca JF, Depukat K, Hallagan JB (1990) Lifetime toxicity/carcinogenicity studies of FD & C Blue No. 1 (brilliant blue FCF) in rats and mice. Food Chem Toxicol 28:221–234

Butt A, Pugh M, Hubbard P, James G (2004) Functions of optic nerve glia: axoglial signaling in physiology and pathology. Eye 18:1110–1121

Cervetto C, Frattaroli D, Maura G, Marcoli M (2013) Motor neuron dysfunction in a mouse model of ALS: gender-dependent effect of P2 × 7 antagonism. Toxicology 311:69–77. https://doi.org/10.1016/j.tox.2013.04.004

Croall DE, Demartino GN (1991) Calcium-activated neutral protease (calpain) system: structure, function, and regulation. Physiol Rev 71:813–847

Deford SM, Wilson MS, Rice AC et al (2002) Repeated mild brain injuries result in cognitive impairment in B6C3F1 mice. J Neurotrauma 19:427–438

Diaz-Hernandez JI, Gomez-Villafuertes R, León-Otegui M et al (2012) In vivo P2 × 7 inhibition reduces amyloid plaques in Alzheimer's disease through GSK3β and secretases. Neurobiol Aging 33:1816–1828. https://doi.org/10.1016/j.neurobiolaging.2011.09.040

Doan N, Patel M, Doan H, Janich K, Nguyen HS, Shabani S (2016) Traumatic brain injury. Int J Phys Med Rehabil 4:120–121. https://doi.org/10.4172/2329-9096.1000e120

Doig RLOH, Chiha W, Giacci M et al (2017) Specific ion channels contribute to key elements of pathology during secondary degeneration following neurotrauma. BMC Neurosci 18:62

Dong X-X, Wang Y, Qin Z-H (2009) Molecular mechanisms of excitotoxicity and their relevance to pathogenesis of neurodegenerative diseases. Acta Pharmacol Sin Acta Pharmacol Sin 30:379–387. https://doi.org/10.1038/aps.2009.24

Donnelly-Roberts DL, Jarvis MF (2007) Discovery of P2 × 7 receptor-selective antagonists offers new insights into P2 × 7 receptor function and indicates a role in chronic pain states. Br J Pharmacol 151:571–579. https://doi.org/10.1038/sj.bjp.0707265

Farooqui AA, Ong W-Y, Horrocks LA (2008) Neurochemical aspects of excitotoxicity. Springer, New York

Fitzgerald M, Bartlett CA, Evill L, Rodger J, Harvey AR, Dunlop SA (2009a) Secondary degeneration of the optic nerve following partial transection: the benefits of lomerizine. Exp Neurol 216:219–230. https://doi.org/10.1016/j.expneurol.2008.11.026

Fitzgerald M, Payne SC, Bartlett CA, Evill L, Harvey AR, Dunlop SA (2009b) Secondary retinal ganglion cell death and the neuroprotective effects of the calcium channel blocker lomerizine. Investig Ophthalmol Vis Sci 50:5456–5462. https://doi.org/10.1167/iovs.09-3717

Fitzgerald M, Bartlett CA, Harvey AR, Dunlop SA (2010a) Early events of secondary degeneration after partial optic nerve transection: an immunohistochemical study. J Neurotrauma 27:439–452

Fitzgerald M, Bartlett CA, Payne SC, Hart NS, Rodger J, Harvey AR, Dunlop SA (2010b) Near infrared light reduces oxidative stress and preserves function in CNS tissue vulnerable to secondary degeneration following partial transection of the optic nerve. J Neurotrauma 27:2107–2119. https://doi.org/10.1089/neu.2010.1426

Fowler J, McCracken E, Dewar D, McCulloch J (2003) Intracerebral injection of AMPA causes axonal damage in vivo. Brain Res 991:104–112. https://doi.org/10.1016/J.BRAINRES.2003.08.004

Fu Y, Wang H, Huff TB, Shi R, Cheng J-X (2007) Coherent anti-Stokes Raman scattering imaging of myelin degradation reveals a calcium-dependent pathway in lyso-PtdCho-induced demyelination. J Neurosci Res 85:2870–2881. https://doi.org/10.1002/jnr.21403

Giacci MK, Bartlett CA, Smith NM et al (2018) Oligodendroglia are particularly vulnerable to oxidative damage after neurotrauma in vivo. J Neurosci 38:1898–1917

Hara H, Shimazawa M, Sasaoka M et al (1999) Selective effects of lomerizine, a novel diphenylmethylpiperazine Ca^{2+} channel blocker, on cerebral blood flow in rats and dogs. Clin Exp Pharmacol Physiol 26:870–876. https://doi.org/10.1046/j.1440-1681.1999.03154.x

Howell OW, Palser A, Polito A et al (2006) Disruption of neurofascin localization reveals early changes preceding demyelination and remyelination in multiple sclerosis. Brain 129:3173–3185. https://doi.org/10.1093/brain/awl290

Jiang L-H, Mackenzie AB, North RA, Surprenant A (2000) Brilliant Blue G selectively blocks ATP-gated rat P2 × 7 receptors. Mol Pharmacol 58:82–88

Khorchid A, Ikura M (2002) How calpain is activated by calcium. Nat Struct Biol 9:239–241. https://doi.org/10.1038/nsb0402-239

Kimbler DE, Shields J, Yanasak N, Vender JR, Dhandapani KM, Kleinschnitz C (2012) Activation of P2 × 7 promotes cerebral edema and neurological injury after traumatic brain injury in mice. PLoS One. https://doi.org/10.1371/journal.pone.0041229

Kwon BK, Okon E, Hillyer J et al (2011) A systematic review of non-invasive pharmacologic neuroprotective treatments for acute spinal cord injury. J Neurotrauma 28:1545–1588

Labiche LA, Grotta JC (2004) Clinical trials for cytoprotection in stroke. NeuroRx 1:46–70. https://doi.org/10.1602/neurorx.1.1.46

Levkovitch-Verbin H, Quigley HA, Martin KRG, Zack DJ, Pease ME, Valenta DF (2003) A model to study differences between primary and secondary degeneration of retinal ganglion cells in rats by partial optic nerve transection. Investig Opthalmol Vis Sci 44:3388–3388. https://doi.org/10.1167/iovs.02-0646

Matute C (2008) P2 × 7 receptors in oligodendrocytes: a novel target for neuroprotection. Mol Neurobiol 38:123–128. https://doi.org/10.1007/s12035-008-8028-x

Maxwell WL (2013) Damage to myelin and oligodendrocytes: a role in chronic outcomes following traumatic brain injury? Brain Sci 3:1374–1394. https://doi.org/10.3390/brainsci3031374

Mirron V, Kuhlmann T, Antel J (2011) Cells of the oligodendroglial lineage, myelination and remyelination. Biochem Biophys Acta 1812:184–193

Ouyang H, Sun W, Fu Y, Li J, Cheng J-X, Nauman E, Shi R (2010) Compression induces acute demyelination and potassium channel exposure in spinal cord. J Neurotrauma 27:1109–1120. https://doi.org/10.1089/neu.2010.1271

Peng W, Cotrina ML, Han X et al (2009) Systemic administration of an antagonist of the ATP-sensitive receptor P2 × 7 improves recovery after spinal cord injury. Proc Natl Acad Sci USA 106:12489–12493

Reimer MM, McQueen J, Searcy L et al (2011) Rapid disruption of axon–glial integrity in response to mild cerebral hypoperfusion. J Neurosci 31:18185–18194. https://doi.org/10.1523/JNEUROSCI.4936-11.2011

Savigni DL, Doig RLOH, Szymanski CR, Bartlett CA, Lozić I, Smith NM, Fitzgerald M (2013) Three Ca^{2+} channel inhibitors in combination limit chronic secondary degeneration following neurotrauma. Neuropharmacology 75:380–390. https://doi.org/10.1016/j.neuropharm.2013.07.034

Shields DC, Deiber GE, Banik NL (1997) Calpain: a mediator of myelin breakdown in demyelinating diseases. Ann N Y Acad Sci 825:128–130. https://doi.org/10.1111/j.1749-6632.1997.tb48422.x

Sun W, Fu Y, Shi Y, Cheng J-X, Cao P, Shi R (2012) Paranodal myelin damage after acute stretch in guinea pig spinal cord. J Neurotrauma 29:611–619. https://doi.org/10.1089/neu.2011.2086

Szymanski CR, Chiha W, Morellini N et al (2013) Paranode abnormalities and oxidative stress in optic nerve vulnerable to secondary degeneration: modulation by 670 nm light treatment. PLoS One. https://doi.org/10.1371/journal.pone.0066448

Takahashi M, Kohara A, Shishikura J-I et al (2002) YM872: a selective, potent and highly water-soluble alpha-amino-3-hydroxy-5-methylisoxazole-4-propionic acid receptor antagonist. CNS Drug Rev 8:337–352

Thorburne S, Juurlink B (1996) Low glutathione and high iron govern the susceptibility of oligodendroglial precursors to oxidative stress. J Neurochem 67:1014–1022

Tomkins O, Feintuch A, Benifla M, Cohen A, Friedman A, Shelef I (2011) Blood-brain barrier breakdown following traumatic brain injury: a possible role in posttraumatic epilepsy. Cardiovasc Psychiatry Neurol 2011:765923. https://doi.org/10.1155/2011/765923

Tymianski M, Charles T (1996) Normal and abnormal calcium homeostasis in neurons: a basis for the pathophysiology of traumatic and ischemic central nervous system injury. Neurosurgery 38:1176–1195

Wang Y-C, Cui Y, Cui J-Z et al (2015) Neuroprotective effects of brilliant blue G on the brain following traumatic brain injury in rats. Mol Med Rep 12:2149–2154. https://doi.org/10.3892/mmr.2015.3607

Wong HE, Qi W, Choi H-M, Fernandez EJ, Kwon I (2011) A safe, blood-brain barrier permeable triphenylmethane dye inhibits amyloid-β neurotoxicity by generating nontoxic aggregates.

ACS Chem Neurosci 2:645–657. https://doi.org/10.1021/cn200056g

Wu D, Miyamoto O, Shibuya S et al (2005) Different expression of macrophages and microglia in rat spinal cord contusion injury model at morphological and regional levels. Acta Med Okayama 59:121–127. https://doi.org/10.18926/AMO/31950

Zetterberg H, Smith DH, Blennow K (2013) Biomarkers of mild traumatic brain injury in cerebrospinal fluid and blood. Nat Rev Neurol 9:201–210. https://doi.org/10.1038/nrneurol.2013.9

Zhang Z, David G (2015) Stimulation-induced Ca^{2+} influx at nodes of Ranvier in mouse peripheral motor axons. J Physiol 594:39–57. https://doi.org/10.1113/JP271207